Nanoscale

Check for updates

Magnetic skyrmions without the skyrmion Hall effect in a magnetic nanotrack with perpendicular anisotropy†

Yue Zhang, Shijiang Luo, Baiqian Yan, Jun Ou-Yang,* Xiaofei Yang, Shi Chen, Benpeng Zhu and Long You [ID] *

Magnetic skyrmions have potential applications in novel information devices with excellent energy efficiency. However, the skyrmion Hall effect (SkHE) could cause skyrmions moving in a nanotrack to get annihilated at the track edge. In this work, we discovered that the SkHE is depressed by modifying the magnetic structure at the edge of a track, and thus the skyrmion can move in almost a straight line at a high speed. Unlike the inner part of a track with perpendicular magnetic anisotropy, the edge layer exhibits in-plane magnetic anisotropy, and the orientation of edge moments is opposite that at the perimeter of skyrmions nearby. As a result, an enhanced repulsive force acts on the skyrmion to oppose the Magnus force that causes the SkHE. Additionally, the Dzyaloshinskii–Moriya interaction (DMI) constant of the edge layer also matters. When there is no DMI at the edge layer, the transverse displacement of the skyrmion can be depressed effectively when the width of the edge layer is sufficiently large. However, when the inner part and the edge share the same DMI constant, non-monotonically varied transverse displacement occurs because of the Néel-wall-like structure at the edge layer.

1. Introduction

Skyrmions were originally introduced as a model in nuclear physics to develop nonlinear field theory for interacting pions and to describe localized, particle-like configurations in the fields of pion particles.[1] A skyrmion is now highly relevant to the spin structure in condensed-matter systems.

Magnetic skyrmions are chiral spin structures with a whirling configuration.[2] Because their structure cannot be continuously deformed to a ferromagnetic or other magnetic state, skyrmions are topologically protected.[3–5] Due to their topologi-

School of Optical and Electronic Information, Huazhong University of Science and Technology, Wuhan, 430074, P.R. China. E-mail: lyou@hust.edu.cn, oyj@hust.edu.cn

†Electronic supplementary information (ESI) available: The simulation method; the initial state for the magnetization distribution of moments at the edge layer; calculation of the skyrmion number Q and the dissipative tensor D_{ij}; the evolution of the displacement and velocity of a skyrmion in the PM track with an edge layer with IMA with different boundary widths under a current of 2.5×10^{11} A m^{-2}; the evolution of the y-component of the Magnus force and that of the edge force with different boundary widths under a current of 2.5×10^{11} A m^{-2}; the transverse displacement dependence of the y-components of the Magnus force and the edge force with different boundary widths under a current of 2.5×10^{11} A m^{-2}; the calculation of the effective field ($\vec{H}_{eff}$); the influence of the thickness dependence of exchange coupling strength. See DOI: 10.1039/c7nr01980g

cal nature, skyrmions are stable against moderate perturbations. As a result, under the effect of spin transfer torque (STT) or spin orbital torque (SOT), a skyrmion can move smoothly in a nano-sized track with defects.[3,5,6] Two key factors that motivate the study of magnetic skyrmions are their ultimate small size (a few to tens of nanometers)[7–11] and the relatively low current density of a small skyrmion in a medium with a good purity,[3,5,12,13] significantly reducing the dissipation and enhancing the energy efficiency in the process of information manipulation. These two factors not only raise interesting fundamental questions about the chiral magnetic order induced by spin–orbit coupling but also open the door to new concepts of ultradense information storage, logic gates, and computing devices.[14–18]

The creation and motion of an isolated magnetic skyrmion in thin films is a key for future skyrmion-electronics applications. Previous numerical simulations have shown that, under the influence of a spin polarized current *via* STT or SOT, isolated skyrmions can be created and manipulated.[3–6] However, when a skyrmion is driven by a spin polarized current, the movements of the skyrmion away from the intended direction can be attributed to the presence of the Magnus force, which arises because of the coupling between the conduction electron spin and the local magnetization.[3,5,6,19] This is referred to as the skyrmion Hall effect (SkHE), which was theoretically proposed by Zang *et al.*[20] and

was experimentally observed recently.[13,21] This deflection is a serious problem in the realization of skyrmion-based devices because it leads to skyrmion annihilation at the film edges after a short traveling distance. This will be a bottleneck in realizing skyrmionic ultradense devices.[22]

Until now, the methods proposed to reduce the SkHE have mostly utilized a spin-wave or magnon to manipulate skyrmions, which is difficult to integrate into a skyrmionic nanocircuit.[23,24] Very recently, authors have proposed current-driven skyrmion motion to suppress the SkHE by using an antiferromagnetically (AFM) exchanged-couple bilayer system[25,26] or local potential barriers to surround and compress the skyrmion in the nanotrack.[27] In the AFM skyrmion system, the Magnus forces of the neighboring skyrmions are counteracted by each other. As a result, both skyrmions can move without deflection under any current. However, this proposal seems to be not quite realistic. Firstly, to obtain the bilayer with AFM coupled skyrmions is challenging in experiments. On the other hand, reading the skyrmions electrically in this bilayer system is not easy due to zero net moment for the whole system.

In this work, to suppress the SkHE, we propose an isolated magnetic skyrmion that is created and driven in a perpendicularly magnetized (PM) nanotrack with an in-plane magnetized (IM) boundary layer outside one side of the track. Due to this edge modification, the transverse displacement of skyrmions is reduced or does not appear. In turn, the skyrmion can be driven without touching the edge under a certain current. The moments in the boundary region point towards the center of the nanotrack, but in the direction opposite to that of the perimeter of the magnetic skyrmion (Fig. 1a). This results in a repulsive force that acts to counteract the Magnus force (Fig. 1b). Our results give guidance for the design and realization of ultradense and ultrafast skyrmion-based memory and logic computing devices with low power consumption.

2. Materials and methods

We investigate a system where a rectangle-shaped PM Co/Pt bilayer is coupled with a boundary layer with effective in-plane
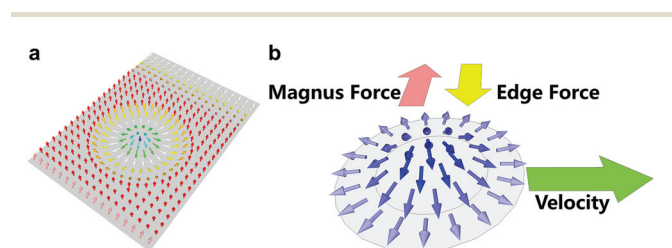
Fig. 1 Schematics of the depression of the SkHE *via* edge modification. (a) The skyrmion in a PM nanotrack with an IM edge layer of a given width. (b) The Magnus force for a moving skyrmion. The Magnus force is cancelled or significantly depressed by the force between the moments at the edge and that at the perimeter of the skyrmion, resulting in the depressed transverse motion of the skyrmion.

magnetic anisotropy (IMA) by means of micromagnetic simulation using the software "Object-Oriented MicroMagnetic Framework" (OOMMF) with code including the Dzyaloshinskii–Moriya interaction (DMI).[28] We assumed that the value of the perpendicular magnetocrystalline anisotropy constant (K_u) for the boundary layer was two orders smaller than that in the PM region. This boundary anisotropy energy was much smaller than the demagnetization energy, ensuring effective in-plane boundary magnetic anisotropy. In experiments, the variation in K_u might have been accompanied by a change in the DMI constant at the boundary (D_b) since both parameters are related to interface atomic coupling. However, it is not easy to estimate it. In our simulation, two marginal values were considered for D_b, which is zero or the same as that in the PM track (here, 3 mJ m^{-2}). The method for the simulation is given in the ESI section S1† in detail.

For the initial state of the PM magnet in the +z-direction, the magnetic moment of the boundary layer with in-plane anisotropy will be aligned in the −y-direction in the equilibrium state by exchange coupling. An isolated skyrmion can be created in this hybrid system composed of the PM nanotrack coupled with or without the IM boundary (see the ESI section S2†).

The movements of the skyrmion away from the intended direction can be understood within the framework of the Thiele equation while assuming the rigidity of the spin textures during the skyrmion motion. In the presence of the spin-Hall effect (SHE) and the interfacial DMI by neglecting the STT contribution, the equation of skyrmion motion can be found:[3,29]

$$\frac{M_S \tau}{\gamma}\left(\vec{G} \times \vec{v} + \alpha \overleftrightarrow{D} \cdot \vec{v}\right) + \vec{F}_{spin} + \vec{F} = 0, \tag{1}$$

Here M_S is the saturation magnetization; γ is the gyromagnetic ratio (a negative value); τ is the thickness of FM films; $\vec{G}$ is the gyrocoupling vector, and $v = \dot{R}'(t)$ (where "." denotes the time derivative) with $v = (v_x, v_y)$ and $R' = (X,Y)$ as the drift velocity and the center position of the magnetic skyrmion, respectively. α is the Gilbert damping coefficient, and $\overleftrightarrow{D}$ is the dissipative tensor, and the D_{ij} components are $D_{xx} = D_{yy} = D$ and 0 otherwise. $\overleftrightarrow{D} = D_{xx}\vec{e}_x\vec{e}_x + D_{yy}\vec{e}_y\vec{e}_y$, and $\vec{e}_x$ and $\vec{e}_y$ are the unit vectors along the x- and y-directions, respectively. $\vec{F}_{spin}$ is the force acting on the skyrmion by the spin current moving perpendicular into the FM film. The skyrmion is driven to move along the track under $\vec{F}_{spin}$. In general, this spin current is generated by the spin Hall effect of the HM layer.

The first term on the left hand side of eqn (1) is the Magnus force, and $\vec{G} = 4\pi Q \vec{e}_z$, where $\vec{e}_z$ is the unit vector along the z-direction and Q is the skyrmion number, which is an integer representing the number of times the spin direction wraps the unit sphere. It is defined by[30]

$$Q = \frac{1}{4\pi}\iint \vec{m} \cdot \left(\frac{\partial \vec{m}}{\partial x} \times \frac{\partial \vec{m}}{\partial y}\right)dxdy, \tag{2}$$

where $\vec{m}$ is a unit vector representing the direction of the moments. The essential difference between the domain wall and the skyrmion is that $Q = 0$ for the domain wall, whereas $Q = \pm1$ for the skyrmion. Because the value of Q of a skyrmion is nonzero, a non-zero Magnus force acts on the skyrmion, and its y-component is

$$(F_M)_y = (4\pi Q v_x)M_S\tau/\gamma, \tag{3}$$

which gives it a transverse velocity. For a topologically protected skyrmion, the absolute value of Q is 1. Therefore, the y-component of the Magnus force is proportional to v_x.

In this work, the force $\vec{F}$, in eqn (1), represents the interaction force between the in-plane magnetic moments in the boundary and that at the perimeter of the skyrmion. Based on the tensor calculation, it is easy to determine that $\vec{F} = F_x\vec{e}_x + F_y\vec{e}_y$ and that F_x and F_y satisfy the following equations:

$$F_x = -\frac{M_S\tau}{\gamma}(-4\pi Q v_y + \alpha D_{xx}v_x) - F_{\text{spin}}, \tag{4}$$

$$F_y = -\frac{M_S\tau}{\gamma}(4\pi Q v_x + \alpha D_{yy}v_y). \tag{5}$$

In a track with a confined geometry, F_y increases with the transverse displacement of the skyrmion.[3] When F_y is increased up to $(F_M)_y$ but acts in the opposite direction, the magnetic skyrmion is in equilibrium under both forces, leading to the stable longitude motion of the skyrmion.

3. Results and discussion

Firstly, we consider the creation of the magnetic skyrmion. We found that, at both D_b of 0 and 3 mJ m^{-2}, a skyrmion with a diameter of about 15 nm can be generated in any track with the boundary width (w_b) varying from 0 nm to 40 nm or even wider (see ESI section S2†). Once the skyrmion is created in the system composed of a PM nanotrack with an IM edge layer, the moments in the boundary region point towards the center of the nanotrack, but in the direction opposite to that of the close outer boundaries of the magnetic skyrmion (see ESI Fig. S1†). In the magnetization equilibrium state, the interaction between the in-plane moments of the boundary layer and that of the skyrmion perimeter exactly counteract the Magnus force. As shown in Fig. 2a, under a current with a density (J) of 5×10^{11} A m^{-2}, the Magnus force exceeds the maximum repulsive force from the edge in the PM nanotrack without an IM boundary, leading to the skyrmion annihilation at the film edges after a short traveling distance. However, in the track with IM edge layers where $D_b = 0$ and 3 mJ m^{-2}, the magnetic skyrmion can be driven by the spin current with the same J in a straight line along the nanotrack without touching its edge by suppressing the Magnus force (Fig. 2b and c).

The relationship between the transverse displacement (Δy) and w_b under different magnitudes of the injected current is
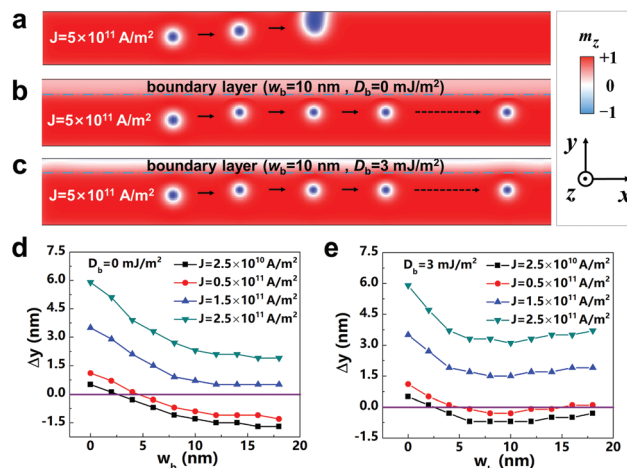
Fig. 2 Current-induced motion of skyrmions in the nanotrack with a boundary layer with IMA. (a) Trajectory of a single skyrmion in a PM track under a current where J is 5×10^{11} A m^{-2}. Trajectory of a single skyrmion in a PM track with an IM edge layer with a DMI constant, D_b, of (b) zero and (c) 3 mJ m^{-2}. Transverse displacement Δy as a function of the boundary width w_b under currents with different J values for D_b values of (d) zero and (e) 3 mJ m^{-2}.

shown in Fig. 2d and e. Firstly, the transverse displacement increases with the magnitude of the injected current. Secondly, the transverse deviation continues to decrease with w_b for D_b values of both zero and 3 mJ m^{-2}, and even the strong repulsive interaction changes the direction of the transverse motion (from $+y$ to $-y$). When D_b is zero, the skyrmion does not move further along the transverse direction with a further increase in the boundary width when the w_b exceeds 10 nm. When D_b is 3 mJ m^{-2} and J is 0.5×10^{11} A m^{-2}, zero Δy appears when w_b is around 5 nm or 15 nm. The disappearance of the transverse deviation means that the Magnus force is completely canceled from the beginning of the motion.

To understand the alteration of the transverse deviation with w_b, the critical mechanism is the competition between two factors: $(F_M)_y$ and F_y. Both forces cooperate in the Thiele equations (eqn (3) and (5)) mentioned above. To determine both forces, four parameters, Q, $D_{xx} = D_{yy}$, v_x, and v_y, must be known. The values of Q and D_{yy} are numerically calculated (see ESI section S3†). v_x and v_y can be simulated (see ESI section S4†).

The addition of the IM edge layer has little influence on the Q of the isolated skyrmion and all the absolute values of Q are very close to 1 (see ESI Fig. S3†). However, the addition of the IM edge has a small impact on D_{yy}, indicating that adding the IM edge influences the local magnetization distribution of the skyrmion but does not change its topological properties. However, the addition of the IM edge influences both the v_x and v_y of the skyrmion before it reaches its final stable motion.

Using eqn (3) and (5) and the Q, D_{yy}, v_x, and v_y values, the evolution of $(F_M)_y$ and F_y within the first 1 ns was determined. Both $(F_M)_y$ and F_y increase monotonically with time (t) under a

current of 2.5×10^{11} A m^{-2} (see ESI Fig. S6†). They are of the order of 10^{-13} N that is consistent with the magnitude (10^{-5} N m^{-1}) estimated by Lin et al.[19] The transverse motion of the skyrmion is not decided by $(F_M)_y$ and F_y, but is attributed to the competition between them. When there is no difference between them, the transverse displacement disappears, and the skyrmion moves strictly along the long side of the track. As shown in Fig. 3a and b, the difference between $(F_M)_y$ and F_y narrows with t and is dependent on w_b. When D_b is zero, the difference between them narrows with an increase in w_b. However, when D_b is 3 mJ m^{-2}, the difference between them is smallest when w_b is 10 nm. This explains the w_b-dependent Δy shown in Fig. 2.

In addition to the time dependence of $(F_M)_y$ and F_y, we also investigated the variation in both forces with w_b. First, we calculated the $(F_M)_y$ and F_y as a function of Δy when the motion of the skyrmion is far from stable. Both $(F_M)_y$ and F_y vary linearly with Δy (see ESI Fig. S7†), which is consistent with the estimation in ref. 3. The linear equations were fitted for both D_b values. Based on the fitted equations, the w_b-dependent F_y and $(F_M)_y$ for different Δy were determined. As a representative example, the w_b-dependence of F_y and $(F_M)_y$ for $\Delta y = 1$ nm is shown in Fig. 4. When $D_b = 0$ mJ m^{-2}, both F_y and $(F_M)_y$ increase with w_b and approach saturation at larger w_b. However, when $D_b = 3$ mJ m^{-2}, both F_y and $(F_M)_y$ change non-monotonically with w_b and reach their maximum when w_b is around 10 nm.

The Magnus force originates from the local interaction between the spin of transported electrons and the moments of the skyrmion.[31] This interaction seems to not rely on the IM edge moments directly. However, it is strictly related to the velocity of the skyrmion, which is affected by adding the IM edge layer. Therefore, the variation in the Magnus force can be understood as follows. The addition of an IM edge changes the transverse velocity of the skyrmion. As a result, as shown in eqn (4), the x-component of the Magnus force is altered. In turn, this variation in the Magnus force influences the longitude velocity of the skyrmion that is proportional to $(F_M)_y$.

To understand the changes in F_y with w_b, the magnetization distribution for the PM nanotrack with an IM edge is depicted in Fig. 5a and b. When no DMI occurs in the boundary layer, the orientation of the moments gradually changes from $+z$ to $-y$. When the w_b is larger than 10 nm, a stable inward tilt of the moments in the boundary layer is formed. When the D_b is 3 mJ m^{-2}, however, the direction of the edge moments changes gradually from $+z$ to $-z$ with w_b increasing from 0 to 18 nm, forming a Néel-type domain wall structure. In this case, the projection of the moment at the y-axis exhibits a non-monotonic change with the coordinate y, and extreme projection appears when w_b is around 10 nm.

It is interesting to see that the change in the edge magnetization distribution with w_b shows a similar trend to the changes in F_y and $(F_M)_y$ with w_b. The physical nature of F_y is the interaction between the effective magnetic field (H_{eff}) of moments at the edge layer and the moments of the skyrmion,[19] and the moments tilting in the $-y$-direction repulse the moments pointing in the $+y$-direction at the perimeter of the skyrmion, resulting in the significantly depressed transverse displacement.[5]

Quantitatively, the force from the track edge can be expressed as:[19]

$$\vec{F} = -\nabla U(\vec{r} - \vec{r}'), \tag{6}$$

where $U(\vec{r} - \vec{r}')$, the interaction potential between a skyrmion at $\vec{r}$ and the edge at $\vec{r}'$, can be expressed as:

$$U(\vec{r} - \vec{r}') = -\int dr''^2 \vec{m}_s(\vec{r} - \vec{r}'') \cdot \vec{H}_{eff}(\vec{r}' - \vec{r}''), \tag{7}$$

where $\vec{m}_s(\vec{r})$ is the local moment of the skyrmion. Without applying an external field, the effective field $\vec{H}_{eff}$ includes the contributions from exchange coupling, DMI, and magnetic anisotropy. Normally, the dipole field is not considered for the skyrmion on the nanometer scale.[32] The $\vec{H}_{eff}$ ascribed to exchange coupling and DMI is relevant to the gradient of a unit vector of magnetic moment in space (see ESI section S7†). However, in a PM nanotrack with a confined boundary, a clear variation of moment orientation only occurs near the edge.[27] Therefore, a large $\vec{H}_{eff}$ exists near the track edge.

From eqn (7), it is also noteworthy that the integral corresponds to integration over the regions that are shared by both the skyrmion and the track edge. Therefore, the edge force is a short-range interaction between the skyrmion and the edge. The force is induced by the overlap between both spin textures.[19] When a skyrmion is so close to the edge the moments
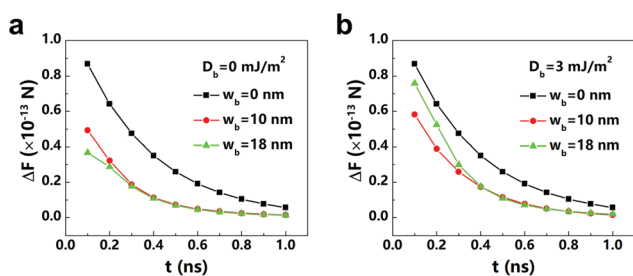

Fig. 3 Evolution of the difference ΔF between the y-component of the Magnus force $(F_M)_y$ and the edge force F_y when (a) $D_b = 0$ mJ m^{-2} and (b) 3 mJ m^{-2}.
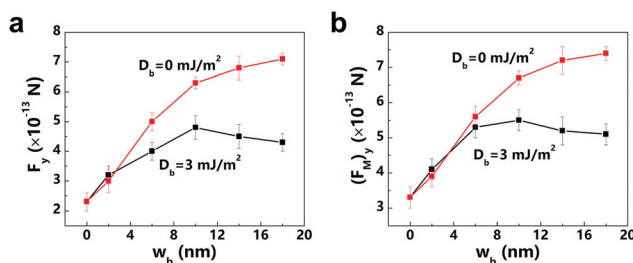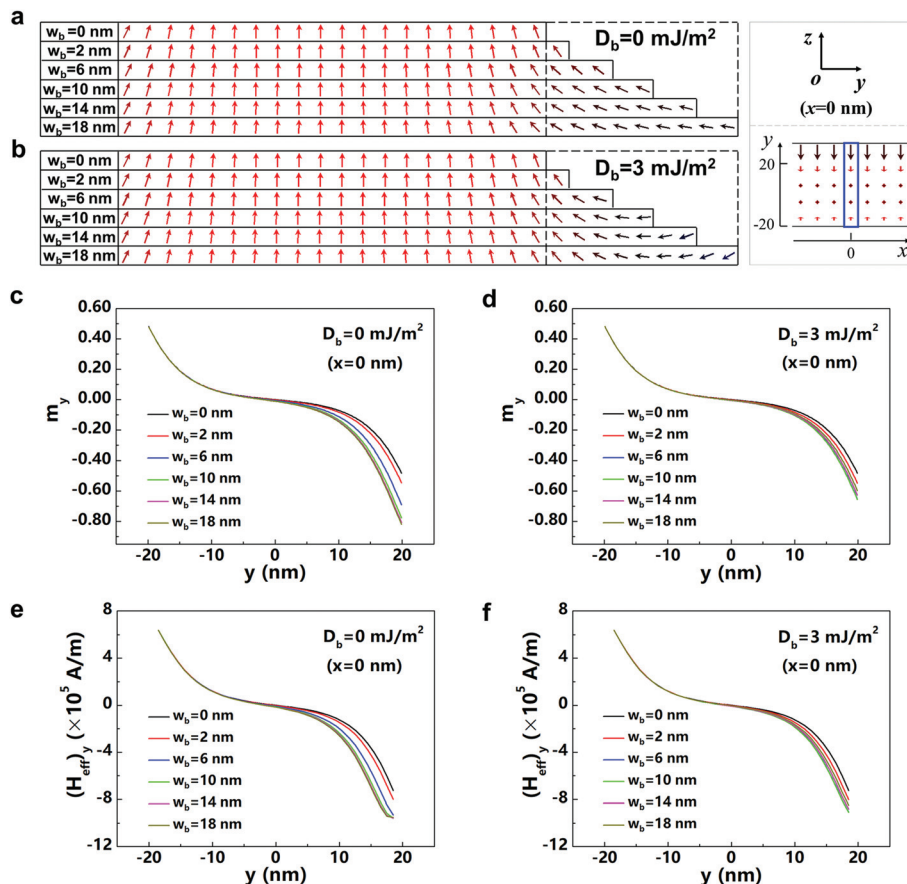

Fig. 4 The boundary width dependence of the y-component of (a) the edge force and (b) the Magnus force for $D_b = 0$ and 3 mJ m^{-2}.

Fig. 5 The magnetization distribution of nanotracks with different boundary widths w_b and a boundary DMI constant D_b of (a) 0 and (b) 3 mJ m^{-2}. The y coordinate dependence of the y-component of the unit vector of moment orientation with different boundary widths w_b and a boundary DMI constant D_b of (c) 0 and (d) 3 mJ m^{-2}. The y coordinate dependence of the y-component of the effective field with different boundary widths w_b and a boundary DMI constant D_b of (e) 0 and (f) 3 mJ m^{-2}.

at its perimeter overlap the nearby moments which is spatially varied. As a result, there will be an edge force acting on the skyrmion.

As depicted in Fig. 5a–d, the addition of the IM edge layers with different D_b and w_b manipulates the spatial variation of the moment orientation near the track edge. When $D_b = 0$ mJ m^{-2}, the increase of w_b expands the area with tilting moments to the inner part of the track. As a result, the region for the edge force also extends to the interior with increasing w_b, resulting in the monotonically varied transverse displacement with w_b. On the other hand, when $D_b = 3$ mJ m^{-2}, the tilting moment spreads to the innermost part when w_b is 10 nm, causing the non-monotonic variation of the transverse displacement with w_b.

Finally, according to eqn (7), the interaction between a skyrmion and the edge also depends on the angle between the neighbor moments at the perimeter of a skyrmion and the $\vec{H}_{\text{eff}}$ near the track edge. At the skyrmion perimeter that is close to the track edge, the net moment orientation is along the $+y$ axis. According to the symmetry of a skyrmion and the orthogonality of the dot product in eqn (7), only the y-component of the effective field $((H_{\text{eff}})_y)$ plays a role in the F_y. Fig. 5e and f

depict that the $(H_{\text{eff}})_y$ varies as a function of y for different D_b and w_b at $x = 0$ nm. The $(H_{\text{eff}})_y(y)$ at other x values is similar to that at $x = 0$ nm. One can see the enhancement of effective field in the $-y$ direction with w_b, and the maximum $(H_{\text{eff}})_y$ for 3 mJ m^{-2} D_b was found when w_b is 10 nm. As a result, the interaction between the moments at the skyrmion perimeter and the effective field was enhanced by the edge modification, which explains the variation of F_y with w_b shown in Fig. 4.

The composite structure of a PM track with an IM edge layer is not difficult to fabricate in experiments. For the Co/Pt bilayer, the IM edge layer can be generated by increasing the thickness of Co near the edge. This can be experimentally realized by an off-axis sputtering to fabricate a wedge in the track and introduce a gradient of magnetic anisotropy constant.[33,34] In this case, the thickness of Co in the edge layer is larger than that in the inner part of the track. Additionally, to some other medium for skyrmions, such as Ta/CoFeB/MgO, this IM edge layer can be formed by reducing the thickness of MgO near the edge *via* Ar ion etching.[35]

In general, the exchange coupling strength depends on the film thickness. On the one hand, the anisotropy constant in the thick edge layer is smaller than that in the inner part of

the track. As a result, a gradual variation of the orientation of magnetic moments occurs in the edge layer, which results in an additional exchange energy that has been considered in resolving the LLG equation. On the other hand, the exchange stiffness constant (A) for nanoscale materials also depends on the film thickness and it may be smaller than that of bulk ones due to the destroyed exchange coupling for the atoms/ions on surfaces.[36,37] Therefore, the A in the boundary layer (A_b) with a thicker ferromagnetic layer may be a little larger than that in the inner part of the track (A_i). The influence of the thickness-dependent A has been carefully discussed in ESI section S8.† It is shown that the large A_b can strengthen the repulsive force from the edge especially when $D_b = 3$ mJ m^{-2}, which is good for reducing the skyrmion Hall effect.

4. Conclusions

To counteract the Magnus force, which results in the SkHE for skyrmions moving in a nanotrack, we added an edge layer with IMA outside one side of the PM track. When the edge DMI is zero, the boundary moments gradually tilt toward the inner part of the track with an increase in the boundary width. The tilted moments at the edge layer repulse the skyrmion, reducing the difference between the Magnus force and the edge force and resulting in the depressed transverse displacement. When the boundary DMI is as large as that in the inner part of the track, however, a Néel-typed domain wall-like magnetization distribution is generated at the edge layer when the boundary width is sufficiently large. This moment structure in the edge layer induces non-monotonic variations in the Magnus force and the edge force, causing a non-monotonic change in the transverse motion of skyrmions. The mechanism is related to the change of the effective field and spatial distribution of tilting moments near the track edge due to the edge modification.

Acknowledgements

References

1 T. H. R. Skyrme, *Nucl. Phys.*, 1962, **31**, 556–569.
2 S. Muhlbauer, B. Binz, F. Jonietz, C. Pfleiderer, A. Rosch, A. Neubauer, R. Georgii and P. Boni, *Science*, 2009, **323**, 915–919.
3 J. Sampaio, V. Cros, S. Rohart, A. Thiaville and A. Fert, *Nat. Nanotechnol.*, 2013, **8**, 839–844.
4 A. Fert, V. Cros and J. Sampaio, *Nat. Nanotechnol.*, 2013, **8**, 152–156.
5 J. Iwasaki, M. Mochizuki and N. Nagaosa, *Nat. Nanotechnol.*, 2013, **8**, 742–747.
6 R. Tomasello, E. Martinez, R. Zivieri, L. Torres, M. Carpentieri and G. Finocchio, *Sci. Rep.*, 2014, **4**, 6784.
7 C. Hanneken, F. Otte, A. Kubetzka, B. Dupe, N. Romming, K. von Bergmann, R. Wiesendanger and S. Heinze, *Nat. Nanotechnol.*, 2015, **10**, 1039–1042.
8 X. Z. Yu, Y. Onose, N. Kanazawa, J. H. Park, J. H. Han, Y. Matsui, N. Nagaosa and Y. Tokura, *Nature*, 2010, **465**, 901–904.
9 S. Woo, K. Litzius, B. Kruger, M. Y. Im, L. Caretta, K. Richter, M. Mann, A. Krone, R. M. Reeve, M. Weigand, P. Agrawal, I. Lemesh, M. A. Mawass, P. Fischer, M. Klaui and G. S. Beach, *Nat. Mater.*, 2016, **15**, 501–506.
10 S. Seki, X. Z. Yu, S. Ishiwata and Y. Tokura, *Science*, 2012, **336**, 198–201.
11 N. Romming, C. Hanneken, M. Menzel, J. E. Bickel, B. Wolter, K. von Bergmann, A. Kubetzka and R. Wiesendanger, *Science*, 2013, **341**, 636–639.
12 W. Jiang, P. Upadhyaya, W. Zhang, G. Yu, M. B. Jungfleisch, F. Y. Fradin, J. E. Pearson, Y. Tserkovnyak, K. L. Wang, O. Heinonen, S. G. E. te Velthuis and A. Hoffmann, *Science*, 2015, **349**, 283–286.
13 G. Yu, P. Upadhyaya, Q. Shao, H. Wu, G. Yin, X. Li, C. He, W. Jiang, X. Han, P. K. Amiri and K. L. Wang, *Nano Lett.*, 2017, **17**, 261–268.
14 W. Kang, Y. Huang, X. Zhang, Y. Zhou and W. Zhao, *Proc. IEEE*, 2016, **104**, 2040–2061.
15 X. Zhang, M. Ezawa and Y. Zhou, *Sci. Rep.*, 2015, **5**, 9400.
16 X. Zhang, Y. Zhou, M. Ezawa, G. P. Zhao and W. Zhao, *Sci. Rep.*, 2015, **5**, 11369.
17 X. Xing, P. W. T. Pong and Y. Zhou, *Phys. Rev. B: Condens. Matter*, 2016, **94**, 054408.
18 G. Finocchio, F. Büttner, R. Tomasello, M. Carpentieri and M. Kläui, *J. Phys. D: Appl. Phys.*, 2016, **49**, 423001.
19 S.-Z. Lin, C. Reichhardt, C. D. Batista and A. Saxena, *Phys. Rev. B: Condens. Matter*, 2013, **87**, 214419.
20 J. Zang, M. Mostovoy, J. H. Han and N. Nagaosa, *Phys. Rev. Lett.*, 2011, **107**, 136804.
21 W. Jiang, X. Zhang, G. Yu, W. Zhang, X. Wang, M. B. Jungfleisch, J. E. Pearson, X. Cheng, O. Heinonen, K. L. Wang, Y. Zhou, A. Hoffmann and S. G. E. te Velthuis, *Nat. Phys.*, 2017, **13**, 162–169.
22 W. Jiang, W. Zhang, G. Yu, M. B. Jungfleisch, P. Upadhyaya, H. Somaily, J. E. Pearson, Y. Tserkovnyak, K. L. Wang, O. Heinonen, S. G. E. te Velthuis and A. Hoffmann, *AIP Adv.*, 2016, **6**, 055602.
23 X. Zhang, M. Ezawa, D. Xiao, G. P. Zhao, Y. Liu and Y. Zhou, *Nanotechnology*, 2015, **26**, 225701.
24 J. Ding, X. Yang and T. Zhu, *IEEE Trans. Magn.*, 2015, **51**, 1–4.
25 X. Zhang, Y. Zhou and M. Ezawa, *Nat. Commun.*, 2016, **7**, 10293.
26 J. Barker and O. A. Tretiakov, *Phys. Rev. Lett.*, 2016, **116**, 147203.
27 I. Purnama, W. L. Gan, D. W. Wong and W. S. Lew, *Sci. Rep.*, 2015, **5**, 10620.
28 S. Rohart and A. Thiaville, *Phys. Rev. B: Condens. Matter*, 2013, **88**, 184422.

29 A. A. Thiele, *Phys. Rev. Lett.*, 1973, **30**, 230–233.

30 N. Nagaosa and Y. Tokura, *Nat. Nanotechnol.*, 2013, **8**, 899–911.

31 T. Schulz, R. Ritz, A. Bauer, M. Halder, M. Wagner, C. Franz, C. Pfleiderer, K. Everschor, M. Garst and A. Rosch, *Nat. Phys.*, 2012, **8**, 301–304.

32 Y. Zhou and M. Ezawa, *Nat. Commun.*, 2014, **5**, 4652.

33 G. Yu, P. Upadhyaya, Y. Fan, J. G. Alzate, W. Jiang, K. L. Wong, S. Takei, S. A. Bender, L. T. Chang, Y. Jiang, M. Lang, J. Tang, Y. Wang, Y. Tserkovnyak, P. K. Amiri and K. L. Wang, *Nat. Nanotechnol.*, 2014, **9**, 548–554.

34 T. J. Klemmer, K. A. Ellis, L. H. Chen, B. van Dover and S. Jin, *J. Appl. Phys.*, 2000, **87**, 830.

35 L. You, O. Lee, D. Bhowmik, D. Labanowski, J. Hong, J. Bokor and S. Salahuddin, *Proc. Natl. Acad. Sci. U. S. A.*, 2015, **112**, 10310–10315.

36 R. H. Kodama, *J. Magn. Magn. Mater.*, 1999, **200**, 359–372.

37 X. Y. Lang, W. T. Zheng and Q. Jiang, *Phys. Rev. B: Condens. Matter*, 2006, **73**, 224444.